

Supplementary information

High Throughput Exploration of the Oxidation Landscape in High Entropy Alloys

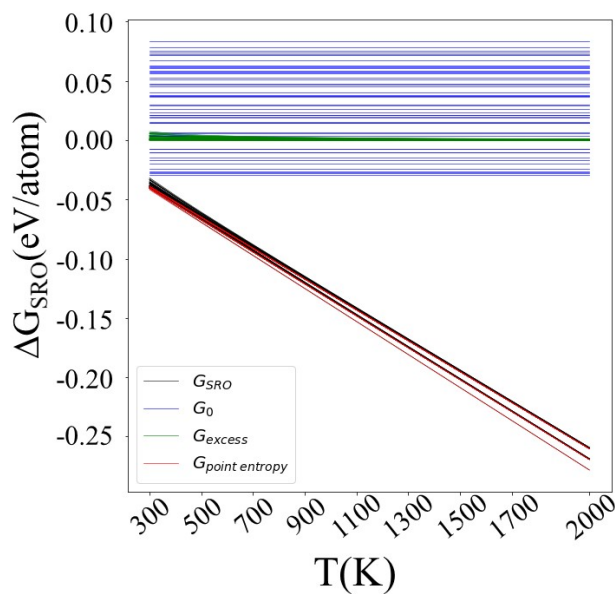
D. Saucedo^a, P. Singh^{a,b}, G. Ouyang,^b O. Palasyuk,^b M. J. Kramer^b, and R. Arroyave ^{a,c}

^a Department of Materials Science & Engineering, Texas A&M University, College Station, TX, 77843, USA

^b Ames Laboratory, United States Department of Energy, Iowa State University, Ames, IA 50011, USA

^c Department of Mechanical Engineering, Texas A&M University, College Station, TX, 77843, USA

Generally, the Bartel model only considers the entropies due to lattice vibrational. As discussed in the Methodology: SRO theory, a main driving force of HEA stability is the configurational entropy captured with the short-range ordering contributions. Therefore, augmenting the Bartel model output, Gibbs Formation energy prediction, by summing it with the additional term Gibbs short-range ordering energy, G_{SRO} , (see Eq. 8 & Eq. 9) accounts for the energy difference.

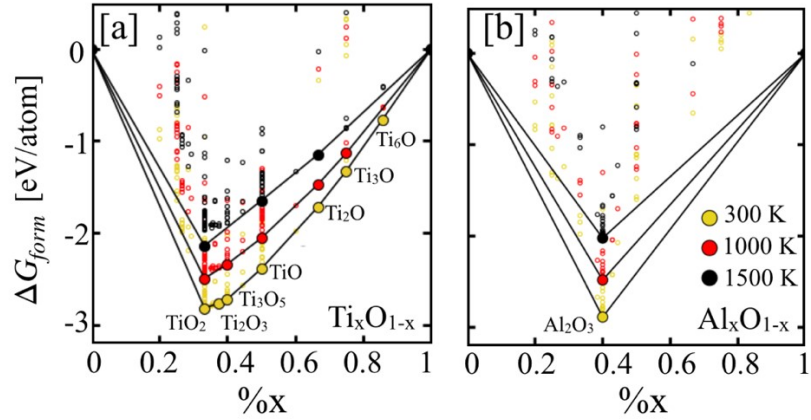


Supplementary Figure 1. The $\Delta G_{\text{form},T}$ with SRO contributions of 51 Mo-W-Ta-Ti-Zr HEAs. We found that small but finite SRO contribution stabilizes the HEA, however, the point-entropy contribution, as expected, wins over SRO at higher temperature.

Here we show the temperature dependent evolution of convex hulls for Ti and Al oxide phases. Our framework was able capture all known experimental phases of Ti-O and Al-O. All the phases are outlined in Table 3. Moreover, we found that these stable phases become pertinent in the overall oxidation analysis.

The predictions for Ti_xO_{1-x} in Fig. 2a are validated against the known experimental phases available on NIST-JANAF thermochemical tables. Our ML framework predicts TiO_2 , Ti_3O_5 , TiO_3 , TiO , Ti_2O , Ti_3O , and Ti_6O as seven stable phases at room temperature (300 K), while Ti_2O and Ti_6O disappear

at high temperature (1500 K) from the hull. On the other hand, only stable $\text{Al}_x\text{O}_{1-x}$ phase in Fig. 2b, i.e., α - Al_2O_3 , remains stable over the tested temperature range (300 K - 1500 K).



Supplementary Figure 2. The convex hull (ΔG_{form}) of (left panel) $\text{Ti}_x\text{O}_{1-x}$, and (right panel) $\text{Al}_x\text{O}_{1-x}$ to provide temperature dependent phase stability of experimentally known oxide phase.

Supplementary Table 1: High Entropy Alloys Ground-state Database

HEA #	Formula [.at%]	dH eV/atom	Volume Ang. ³ /atom	Energy eV/atom	HEA #	Formula [.at%]	dH eV/atom	Volume Ang. ³ /atom	Energy eV/atom
HEA 0	Mo0.2Ta0.2Ti0.2W0.2Zr0.2	0.0271	17.667	-10.3938	HEA 26	Mo.3Ta.3Ti.1W.2 Zr.1	-0.0155	17.106	-11.0624
HEA 1	Mo0.2Ta0.2Ti0.2W0.3Zr0.1	-0.0094	16.962	-10.8714	HEA 27	Mo.3Ta.3Ti.1W.1 Zr.2	0.0203	17.798	-10.5856
HEA 2	Mo0.2Ta0.2Ti0.2W0.1Zr0.3	0.0575	18.466	-9.9224	HEA 28	Mo.3Ta.1Ti.2W.2 Zr.2	0.0234	17.348	-10.2963
HEA 3	Mo0.2Ta0.2Ti0.3W0.2Zr0.1	-0.0064	17.121	-10.3622	HEA 29	Mo.3Ta.1Ti.2W.3 Zr.1	-0.0266	16.713	-10.7873
HEA 4	Mo0.2Ta0.2Ti0.3W0.1Zr0.2	0.0379	17.882	-9.8768	HEA 30	Mo.3Ta.1Ti.2W.1 Zr.3	0.0403	18.096	-9.8383
HEA 5	Mo0.2Ta0.2Ti0.1W0.2Zr0.3	0.0617	18.258	-10.4244	HEA 31	Mo.3Ta.1Ti.3W.2 Zr.1	-0.0267	16.857	-10.2812
HEA 6	Mo0.2Ta0.2Ti0.1W0.3Zr0.2	0.031	17.488	-10.8962	HEA 32	Mo.3Ta.1Ti.3W.1 Zr.2	0.0153	17.545	-9.7982
HEA 7	Mo0.2Ta0.3Ti0.2W0.2Zr0.1	-0.0062	17.261	-10.7581	HEA 33	Mo.3Ta.1Ti.1W.2 Zr.3	0.059	17.915	-10.3259
HEA 8	Mo0.2Ta0.3Ti0.2W0.1Zr0.2	0.0386	17.973	-10.2723	HEA 34	Mo.3Ta.1Ti.1W.3 Zr.2	0.0216	17.192	-10.8043
HEA 9	Mo0.2Ta0.3Ti0.3W0.1Zr0.1	0.0075	17.422	-10.2382	HEA 35	Mo.1Ta.2Ti.2W.2 Zr.3	0.0683	18.484	-10.1228
HEA 10	Mo0.2Ta0.3Ti0.1W0.2Zr0.2	0.0305	17.742	-10.7867	HEA 36	Mo.1Ta.2Ti.2W.3 Zr.2	0.0487	17.681	-10.5834
HEA 11	Mo0.2Ta0.3Ti0.1W0.3Zr0.1	-0.0226	17.11	-11.2808	HEA 37	Mo.1Ta.2Ti.3W.2 Zr.2	0.0592	17.873	-10.0667
HEA 12	Mo0.2Ta0.3Ti0.1W0.1Zr0.3	0.0574	18.572	-10.3187	HEA 38	Mo.1Ta.2Ti.3W.3 Zr.1	0.0051	17.144	-10.5618
HEA 13	Mo0.2Ta0.1Ti0.2W0.2Zr0.3	0.0624	18.093	-10.0275	HEA 39	Mo.1Ta.2Ti.3W.1 Zr.3	0.0845	18.67	-9.6004

HEA 14	Mo0.2Ta0.1Ti0.2W0.3Zr0.2	0.0371	17.354	-10.4939	HEA 40	Mo.1Ta.2Ti.1W.3 Zr.3	0.0739	18.228	-10.6235
HEA 15	Mo0.2Ta0.1Ti0.3W0.2Zr0.2	0.0219	17.582	-10.0028	HEA 41	Mo.1Ta.3Ti.2W.2 Zr.2	0.0399	18.005	-10.4822
HEA 16	Mo0.2Ta0.1Ti0.3W0.3Zr0.1	-0.0094	16.813	-10.4751	HEA 42	Mo.1Ta.3Ti.2W.3 Zr.1	0.0081	17.26	-10.9551
HEA 17	Mo0.2Ta0.1Ti0.3W0.1Zr0.3	0.0633	18.305	-9.5204	HEA 43	Mo.1Ta.3Ti.2W.1 Zr.3	0.0766	18.788	-10.0045
HEA 18	Mo0.2Ta0.1Ti0.1W0.3Zr0.3	0.0633	17.918	-10.5329	HEA 44	Mo.1Ta.3Ti.3W.2 Zr.1	0.0165	17.445	-10.4405
HEA 19	Mo0.3Ta0.2Ti0.2W0.2Zr0.1	-0.0195	16.935	-10.6702	HEA 45	Mo.1Ta.3Ti.3W.1 Zr.2	0.0527	18.216	-9.9632
HEA 20	Mo0.3Ta0.2Ti0.2W0.1Zr0.2	0.0191	17.668	-10.1906	HEA 46	Mo.1Ta.3Ti.1W.2 Zr.3	0.0735	18.548	-10.5139
HEA 21	Mo0.3Ta0.2Ti0.3W0.1Zr0.1	-0.0294	17.132	-10.1738	HEA 47	Mo.1Ta.3Ti.1W.3 Zr.2	0.0475	17.79	-10.9809
HEA 22	Mo0.3Ta0.2Ti0.1W0.2Zr0.2	0.0152	17.499	-10.7008	HEA 48	Mo.1Ta.1Ti.2W.3 Zr.3	0.0749	18.12	-10.2262
HEA 23	Mo0.3Ta0.2Ti0.1W0.3Zr0.1	-0.0269	16.844	-11.1839	HEA 49	Mo.1Ta.1Ti.3W.2 Zr.3	0.0792	18.344	-9.7157
HEA 24	Mo0.3Ta0.2Ti0.1W0.1Zr0.3	0.0531	18.249	-10.2219	HEA 50	Mo.1Ta.1Ti.3W.3 Zr.2	0.0484	17.516	-10.1876
HEA 25	Mo0.3Ta0.3Ti0.2W0.1Zr0.1	-0.0136	17.254	-10.5543					

Supplementary Table 2: The AUC² scoring metrics for each elemental dominate cluster

Mo-Rich			Ta-Rich			Ti-Rich		
	Formula	AUC ²		Formula	AUC ²		Formula	AUC ²
HEA 30	Mo15Ta5Ti10W5Zr15	4216	HEA 0	Mo10Ta10Ti10W10Zr10	3458	HEA 17	Mo10Ta5Ti15W5Zr15	4378
HEA 32	Mo15Ta5Ti15W5Zr10	4001	HEA 45	Mo5Ta15Ti15W5Zr10	3453	HEA 15	Mo10Ta5Ti15W10Zr10	4075
HEA 21	Mo15Ta10Ti15W5Zr5	3799	HEA 12	Mo10Ta15Ti5W5Zr15	3381	HEA 32	Mo15Ta5Ti15W5Zr10	4001
HEA 24	Mo15Ta10Ti5W5Zr15	3727	HEA 43	Mo5Ta15Ti10W5Zr15	3299	HEA 21	Mo15Ta10Ti15W5Zr5	3799
HEA 20	Mo15Ta10Ti10W5Zr10	3701	HEA 25	Mo15Ta15Ti10W5Zr5	3163	HEA 4	Mo10Ta10Ti15W5Zr10	3728
HEA 31	Mo15Ta5Ti15W10Zr5	3670	HEA 9	Mo10Ta15Ti15W5Zr5	3137	HEA 50	Mo5Ta5Ti15W15Zr10	3720
HEA 33	Mo15Ta5Ti5W10Zr15	3571	HEA 8	Mo10Ta15Ti10W5Zr10	3118	HEA 31	Mo15Ta5Ti15W10Zr5	3670
HEA 28	Mo15Ta5Ti10W10Zr10	3509	HEA 11	Mo10Ta15Ti5W15Zr5	3115	HEA 37	Mo5Ta10Ti15W10Zr10	3607
HEA 0	Mo10Ta10Ti10W10Zr10	3458	HEA 41	Mo5Ta15Ti10W10Zr10	3112	HEA 3	Mo10Ta10Ti15W10Zr5	3592
HEA 19	Mo15Ta10Ti10W10Zr5	3452	HEA 26	Mo15Ta15Ti5W10Zr5	3099	HEA 38	Mo5Ta10Ti15W15Zr5	3482
HEA 22	Mo15Ta10Ti5W10Zr10	3351	HEA 44	Mo5Ta15Ti15W10Zr5	3004	HEA 0	Mo10Ta10Ti10W10Zr10	3458
HEA 25	Mo15Ta15Ti10W5Zr5	3163	HEA 7	Mo10Ta15Ti10W10Zr5	2975	HEA 45	Mo5Ta15Ti15W5Zr10	3453
HEA 26	Mo15Ta15Ti5W10Zr5	3099	HEA 46	Mo5Ta15Ti5W10Zr15	2890	HEA 16	Mo10Ta5Ti15W15Zr5	3452
HEA 23	Mo15Ta10Ti5W15Zr5	3055	HEA 10	Mo10Ta15Ti5W10Zr10	2812	HEA 49	Mo5Ta5Ti15W10Zr15	3406
HEA 29	Mo15Ta5Ti10W15Zr5	3021	HEA 27	Mo15Ta15Ti5W5Zr10	2804	HEA 9	Mo10Ta15Ti15W5Zr5	3137
HEA 34	Mo15Ta5Ti5W15Zr10	3017	HEA 47	Mo5Ta15Ti5W15Zr10	2756	HEA 39	Mo5Ta10Ti15W5Zr15	3072
HEA 27	Mo15Ta15Ti5W5Zr10	2804	HEA 42	Mo5Ta15Ti10W15Zr5	2606	HEA 44	Mo5Ta15Ti15W10Zr5	3004
W-Rich			Zr-Rich					
	Formula	AUC2		Formula	AUC2			
HEA 50	Mo5Ta5Ti15W15Zr10	3720	HEA 17	Mo10Ta5Ti15W5Zr15	4378			

HEA 18	Mo10Ta5Ti5W15Zr15	3500	HEA 30	Mo15Ta5Ti10W5Zr15	4216
HEA 38	Mo5Ta10Ti15W15Zr5	3482	HEA 13	Mo10Ta5Ti10W10Zr15	3953
HEA 0	Mo10Ta10Ti10W10Zr10	3458	HEA 2	Mo10Ta10Ti10W5Zr15	3872
HEA 16	Mo10Ta5Ti15W15Zr5	3452	HEA 24	Mo15Ta10Ti5W5Zr15	3727
HEA 48	Mo5Ta5Ti10W15Zr15	3422	HEA 5	Mo10Ta10Ti5W10Zr15	3709
HEA 36	Mo5Ta10Ti10W15Zr10	3369	HEA 33	Mo15Ta5Ti5W10Zr15	3571
HEA 14	Mo10Ta5Ti10W15Zr10	3317	HEA 35	Mo5Ta10Ti10W10Zr15	3518
HEA 1	Mo10Ta10Ti10W15Zr5	3275	HEA 18	Mo10Ta5Ti5W15Zr15	3500
HEA 40	Mo5Ta10Ti5W15Zr15	3194	HEA 0	Mo10Ta10Ti10W10Zr10	3458
HEA 6	Mo10Ta10Ti5W15Zr10	3159	HEA 48	Mo5Ta5Ti10W15Zr15	3422
HEA 11	Mo10Ta15Ti5W15Zr5	3115	HEA 49	Mo5Ta5Ti15W10Zr15	3406
HEA 23	Mo15Ta10Ti5W15Zr5	3055	HEA 12	Mo10Ta15Ti5W5Zr15	3381
HEA 29	Mo15Ta5Ti10W15Zr5	3021	HEA 43	Mo5Ta15Ti10W5Zr15	3299
HEA 34	Mo15Ta5Ti5W15Zr10	3017	HEA 40	Mo5Ta10Ti5W15Zr15	3194
HEA 47	Mo5Ta15Ti5W15Zr10	2756	HEA 39	Mo5Ta10Ti15W5Zr15	3072
HEA 42	Mo5Ta15Ti10W15Zr5	2606	HEA 46	Mo5Ta15Ti5W10Zr15	2890

Supplementary Discussion 1: The AUC² score derivation for the HEA 0, oxide phases, and Intermetallics scores.

In this section, we demonstrate the analytics of determining the AUC² scores of the desired HEA 0 as well as the corresponding decomposing oxide and intermetallic phases that occur as a result of increasing temperature and oxygen content. Consider Figure 5, Figure 10, and Figure 13 from the main text. Recall that Figure 5 is a phase landscape view where the color hue corresponds to fractional amount of a particular phase. The objective is to show that the entirety of Figure 5 can be reviewed as a single row in Figure 15.

Therefore, we write the AUC² of a single phase as the following:

$$AUC^2 \text{ of } A = \int_0^{\max\{n_o\}} \int_{300}^{\max\{T\}} X_A(T, n_o) dndT$$

Here, n_o is the particular moles of oxygen provided to the reservoir, where its maximal amount, $\max\{n_o\}$, is the outer upper integral bound, and where T is temperature.

As an example, we will use Ti2O, TiO, TiO₂, TaMo, TaW, and HEAO. The phase fraction data generated

are discrete points, therefore we analytically solve the oxygen integral $AUC_{XA} = \int_0^{\max\{n_o\}} X_A(T, n_o) dn$ with the `sklearn.metrics.auc function`. Resulting in the following table of values.

Supplementary Table 3: The AUC scores of selected phases

T[K]	Ti2O1	Ti1O1	Ti1O2	Ta1Mo1	Ta1W1	HEAO
------	-------	-------	-------	--------	-------	------

300	4.4549	1.7676	12.5742	12.5592	0.0000	0.0000
400	4.4549	1.7676	12.3247	12.3662	0.0000	0.0000
500	4.4549	1.7676	12.3247	12.2161	0.0000	0.0000
600	4.4549	1.7676	12.3247	12.0811	0.0000	0.0000
700	5.6276	1.7676	11.7661	11.9917	0.0000	0.7326
800	4.9785	1.7676	11.7661	7.1847	0.0000	2.4552
900	4.9785	1.7676	11.9594	7.1847	0.0000	2.4552
1000	4.9785	1.7676	11.9594	7.1847	0.0000	2.4552
1100	4.9785	1.7676	11.9594	7.1847	0.0000	2.4552
1200	0.0000	10.0136	11.9594	6.3292	0.0000	2.6095
1300	0.0000	10.0136	13.7407	0.0000	6.3292	2.6095
1400	0.0000	10.0136	13.7407	0.0000	6.3292	2.6095
1500	0.0000	10.0136	12.4313	0.0000	6.3292	2.6095
1600	0.0000	10.0136	14.0474	0.0000	6.3292	2.6095
1700	0.0000	0.0000	14.0474	0.0000	7.5726	3.4342
1800	0.0000	0.0000	14.0474	0.0000	7.5726	3.4342
1900	0.0000	0.0000	14.0474	0.0000	12.2918	2.7423
2000	0.0000	0.0000	14.0474	0.0000	12.2918	2.7423

Consider the Ti-O chemical system phases, the Ti_2O , TiO , and TiO_2 represent magnelli phases of increasing oxide weight fraction relative to their metallic counterpart. From the three columns we observe that at lower temperatures, metallic heavy oxides are thermodynamically favorable evident by their greater AUC score. However, as temperature increases these oxides fall away in favor of more stable, oxide dense relatives.

Next consider the intermetallic phases, $TaMo$ is present at low temperatures but slowly disappears at increasing temperature while TaW begins to form at similar rate. This informs that TaW is more effective at reducing energy at high temperatures but is virtually non-existent at low temperatures. Finally, is the desired $HEAO$ which has zero formation to 600K and steadily increase formation after that point as graphically represented in Figure 10 in the main text.

$$AUC_{XA}^2 = \int_0^{\max\{T\}} AUC_{XA}(T) dt$$

Completing the second Integral over the temperature space gives the final AUC² result of each discussed phase.

Supplementary Table 4: The AUC² scores of selected phases

Phase	AUC ²
Ti_2O_1	4113.371
Ti_1O_1	6509.274
Ti_1O_2	21775.7
Ta_1Mo_1	9000.253
Ta_1W_1	5889.969
$HEAO$	3458.265

These numerical values are a rapid means to compare across the different HEA candidates shown graphically in Figure 13 and illustrate that certain HEA compositions will have more or less than others and yield varying amounts of competing intermetallic and oxide phases.

Supplementary Table 3: The AUC scores of selected phases

Compound	Prototype	Space group
TiO ₂	Reutile	<i>P</i> 4 ₂ / <i>mnm</i>
Ti ₂ O ₃	α -Al ₂ O ₃	<i>R</i> ̄3 <i>c</i>
Ti ₃ O ₅	Anosovite	<i>C</i> 2/ <i>m</i>
TiO	NaCl	<i>F</i> m̄3 <i>m</i>
Ti ₂ O	Anti-CdI ₂	<i>P</i> ̄3 <i>m</i> 1
Ti ₃ O	Ti ₃ O	<i>P</i> 312
Ti ₆ O	Ti ₆ O	<i>P</i> ̄3 <i>I</i> c
α -Al ₂ O ₃	α -Al ₂ O ₃	<i>R</i> ̄3 <i>c</i>